# Effect of Microstructure on the Heat Affected Zone Toughness of High Nitrogen Containing Ni-Free Austenitic Stainless Steel†

Insu WOO*, Tsutomu HORINOUCHI** and Yasushi KIKUCHI ***

**Abstract**

*This work was undertaken to examine the influence of Cr-nitride on impact property in heat-affected zone of high nitrogen containing Ni-free austenitic stainless steel. Cr-nitride precipitation of HAZ was simulated using the isothermal test and the Gleeble test by varying holding time and cooling rate, respectively. Impact toughness was determined by testing Charpy V-notch type impact specimens (55 × 10 × 5 mm) between room temperature and 77K. Isothermal test results showed that the nose of each C curve (i.e., intergranular, cellular, and transgranular $Cr_2N$) was around 1173K. $Cr_2N$ precipitation occurred sequentially at grain boundaries, by cellular precipitation, and, finally, by transgranular precipitation within the matrix. The amount of intergranular and cellular $Cr_2N$ precipitation increased with increasing holding time or decreasing cooling rate. High nitrogen containing Ni-free austenitic stainless steel exhibited excellent impact toughness at room temperature. At cryogenic temperatures, the value of absorbed energy was decreased markedly, and ductile-to-brittle (DBT) transition behavior associated with brittle transgranular fracture was observed. Intergranular and cellular $Cr_2N$ precipitation reduced impact property of HAZ at room temperature. In addition, embrittlement occurred due to grain boundary separation and fracture through cellular precipitation regions, initiated by $Cr_2N$. However, regardless of intergranular and cellular $Cr_2N$ precipitation, impact toughness values of HAZ were not observed at cryogenic temperatures.*

**KEY WORDS:** (High nitrogen containing Ni-free austenitic stainless steel) ($Cr_2N$) (Charpy V-notch test)) (Charpy Absorbed Energy) (HAZ toughness) (ductile-to-brittle transition)

## 1. Introduction

Structural materials must offer properties such as non-magnetic behavior, high resistance to corrosion and wear, high strength with high toughness according to the demands of the electronics, the precision and the cryogenic industries. High nitrogen containing Ni-free austenitic stainless steels have been developed as modified Cr-Ni austenitic stainless steels because of the saving of nickel resources and material costs. N is known to increase yield strength effectively without concomitant losses of toughness and ductility. Besides these characteristics, N is beneficial in the pitting corrosion resistance of stainless steels, and enhances austenite stability with respect to deformation-induced martensite formation[1-4].

On the other hand, a wider expansion in the use of high nitrogen containing Ni-free austenitic stainless steels is, apart from other features, dependent on their joining characteristics. Little research, however, has been focused on the weldablility of this alloy[5-7]. Although the solubility of N is greater than the solubility of carbon, high nitrogen containing Ni-free austenitic stainless steels are susceptible to nitride precipitation during welding or heat treatment[8-11]. The presence of nitrides has been shown to be detrimental to the mechanical properties of nitrogen containing austenitic stainless steels, however, no systematic study has been conducted in the past.

The objective of the current work was to determine the effect of Cr-nitride on the impact property in the heat-affected zone of high nitrogen containing Ni-free austenitic stainless steel. Cr-nitride precipitation of HAZ was simulated using the isothermal test and the Gleeble test by varying holding time and cooling rate, respectively. The Cr-nitride precipitation behavior of high nitrogen containing Ni-free austenitic stainless steel during heat treatment as well as mechanisms of crack nucleation and fracture, are discussed and related to the

† Received on May 31, 2001
* Post doctoral research fellow
** Technical assistant
*** Professor

Transactions of JWRI is published by Joining and Welding Research Institute of Osaka University, Ibaraki, Osaka 567-0047, Japan.

microstructure.

## 2. Materials and Experimental Procedures

The chemical composition of the high nitrogen containing Ni-free austenitic stainless steel used in the present study is shown in **Table 1**. The material was melted in a high frequency induction melting furnace as a 50kg ingot. A section of the billet was forged at approximately 1473K to produce a billet with a square cross section of 30 × 130 × 200mm. The billet was reheated at 1473K and then hot-rolled without further reheating to produce a 6 × 120 × 1000mm. Solution annealing at 1373K for 1.8ks followed by water quenching ensured that all nitrogen present in the material was dissolved interstitially. As-quenched specimens were confirmed to be of austenitic single phase by X-ray diffraction (XRD) pattern analyses.

Cr-nitride precipitation of HAZ was simulated using the isothermal test and the Gleeble test by varying holding time or cooling rate, respectively. Impact toughness was determined by testing Charpy V-notch type impact specimens (55 × 10 × 5 mm) between room temperature and 77K. The specimens were tested at room temperature and 77K in three-point bending under a bending radius (R=20), a bending angle (180°), using an Instron type testing machine. The shapes of Charpy impact test specimens and three-point bending test specimens are schematically illustrated in **Fig.1 (a)** and **(b)**, respectively.

Microstructural observations of as-received and heat treated specimens were made by scanning electron microscopy (SEM). The specimens were first mechanically polished with emery paper and then etched at 10V × 1 5 sec at room temperature in an aqueous 10% oxalic acid solution. The Cr-nitride precipitation was identified using an energy-dispersive X-ray spectrometer (EDS) attached to transmission electron microscopy (TEM) at 200kV. The TEM thin films were prepared by initial polishing with emery paper, followed by electrojet polishing in alcohol 20% perchloric acid solution at 273K and an electrolytic voltage of 15V.

The linear fraction of intergranular $Cr_2N$ and area fraction of cellular $Cr_2N$ were evaluated by the following relationship through measurement of the total grain boundary length ($\sum L_g$), the total intergranular $Cr_2N$ length ($\sum L_{gn}$), the total view area ($\sum L_a$), and the total cellular $Cr_2N$ area ($\sum L_{ac}$) at 1000-fold magnification:

$$\text{Linear fraction of intergranular } Cr_2N\ (\%) = (\sum L_{gn} / \sum L_g) \times 100$$

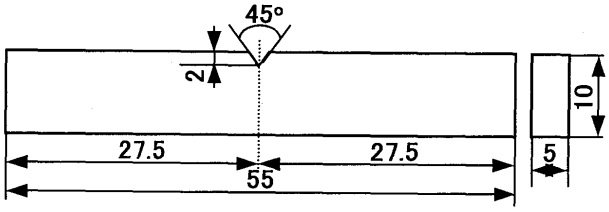


(a) Specimen used for Charpy V-notch impact test

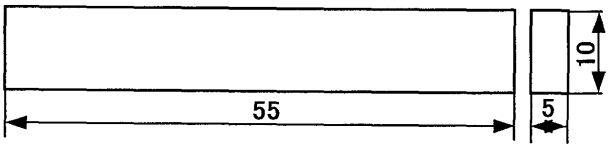


(b) Specimen used for three bending test

Fig.1 Schematic illustration of specimens used for the Charpy V-notch impact test and the three point bending test.

$$\text{Area fraction of cellular } Cr_2N\ (\%) = (\sum L_{ac} / \sum L_a) \times 100$$

## 3. Results

### 3.1 Microstructures of as-received and heat treated materials

**Fig.2** shows SEM micrographs taken from the as-received specimen as well as specimens aged at 1173K for various times. As compared with the microstructure before the heat treatment shown in Fig.2 (a), the amount of white-colored phase present at the grain boundaries and within grains shows an increasing pattern of after the aging treatment (Fig.2 (b) and (c)). It can also be seen from Fig.2 (b) and (c) that cellular precipitates nucleated at grain boundaries and grew into grains. Cellular precipitation products formed in the high nitrogen containing Ni-free austenitic stainless steel have a morphology which is very similar to pearlite formed in carbon steels. **Fig.3** shows TEM micrographs of intergranular, cellular and transgranular precipitate in specimens aged at 1173K for 3.6ks. The electron diffraction analysis revealed that the intergranular, cellular and transgranular precipitate are $Cr_2N$ (Hexagonal, a=0.48113nm, c=0.44841nm). On the other hand, $Cr_2N$ precipitation showed that the nose of each C curve (i.e., intergranular, cellular, and transgranular $Cr_2N$) was around 1173K. $Cr_2N$ precipitation at holding temperature of 1173K occurred sequentially at grain boundaries, by cellular precipitation, and, finally, by transgranular precipitation within the matrix.

Table 1 Chemical composition of high nitrogen containing Ni-free austenitic stainless steel.

| C | Si | Mn | P | S | Ni | Cr | Cu | Mo | V | Al | N | O |
|---|---|---|---|---|---|---|---|---|---|---|---|---|
| 0.043 | 0.43 | 19.92 | 0.004 | 0.006 | 0.01 | 19.60 | 0.01 | 0.01 | 0.01 | <0.005 | 0.746 | 0.0097 |

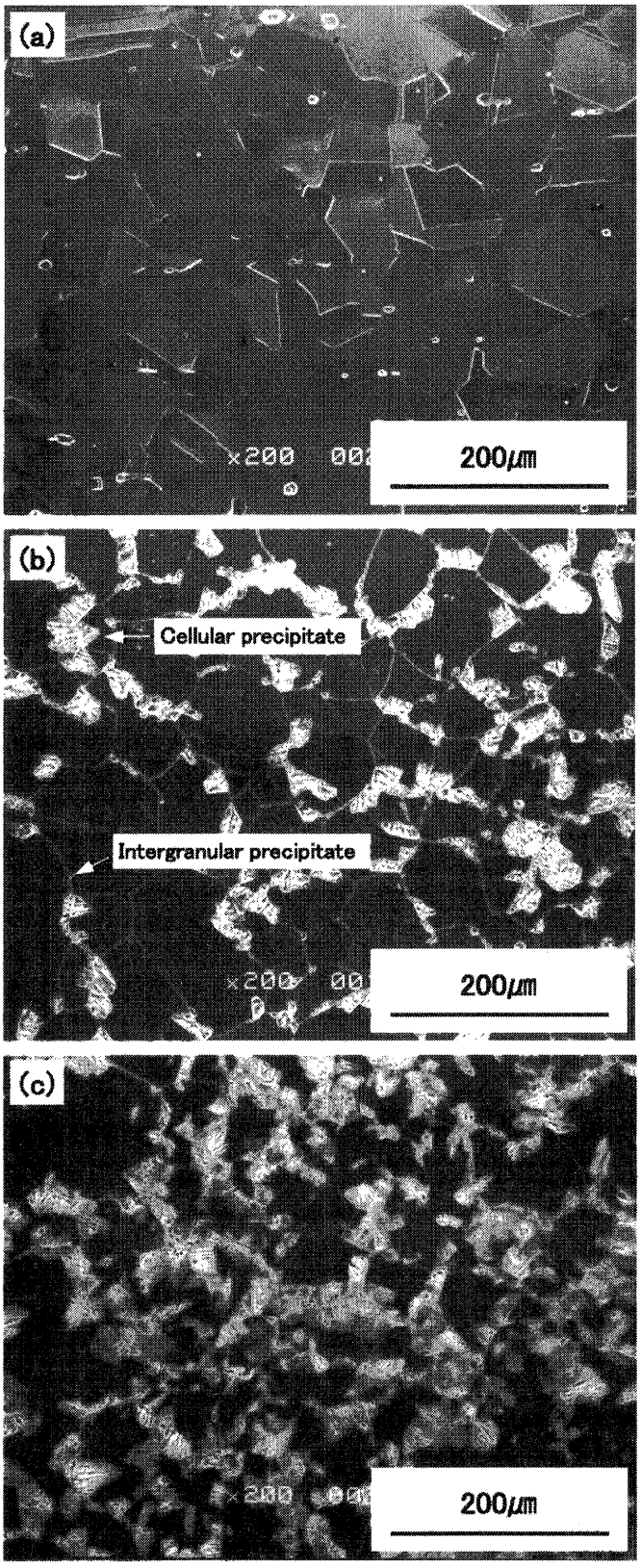


Fig.2 SEM micrographs of base material and aged specimens: (a) Specimen before aging, (b) Specimen aged for 3.6ks at 1173K, (c) Specimen aged for 10.8ks at 1173K.

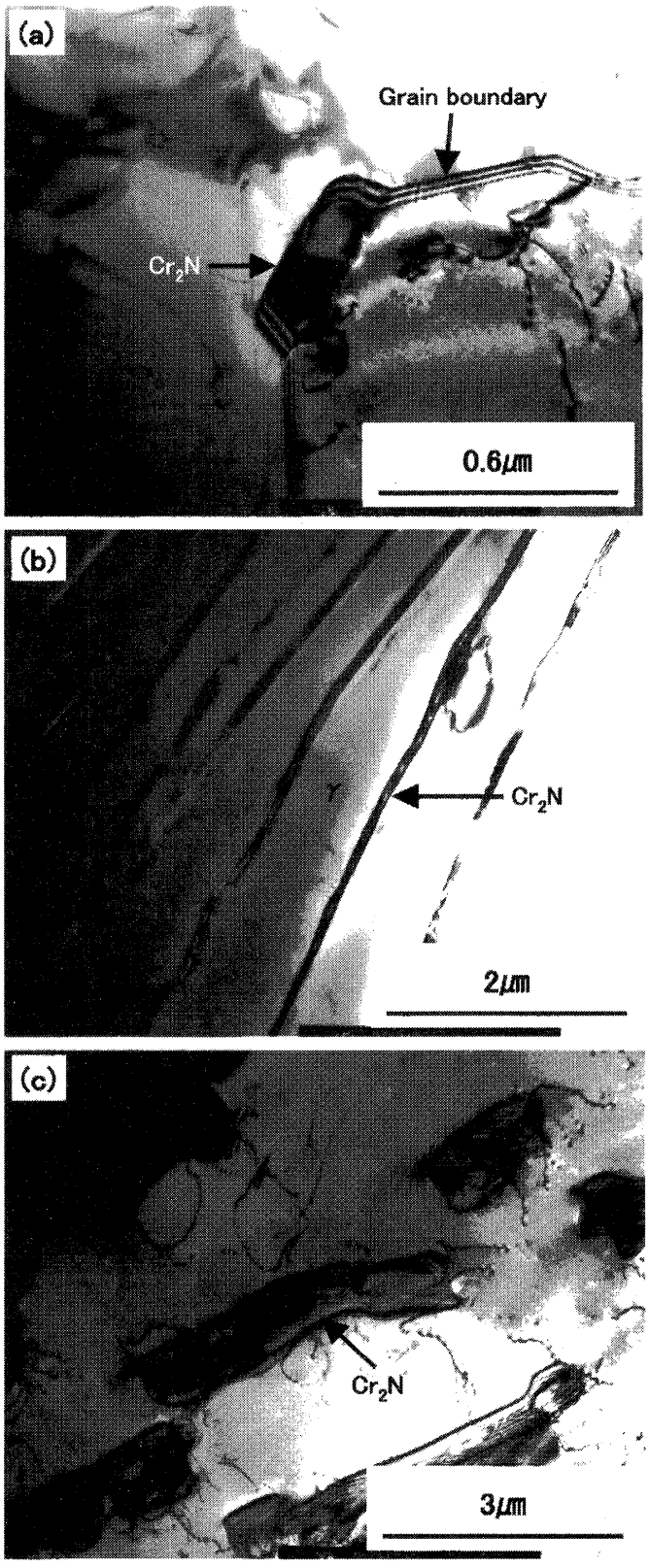


Fig.3 TEM micrographs showing intergranular, cellular and transgranular $Cr_2N$observed in specimens aged for 3.6 ks at 1173K: (a) Intergranular $Cr_2N$, (b) Cellular $Cr_2N$, (c) Transgranular $Cr_2N$.

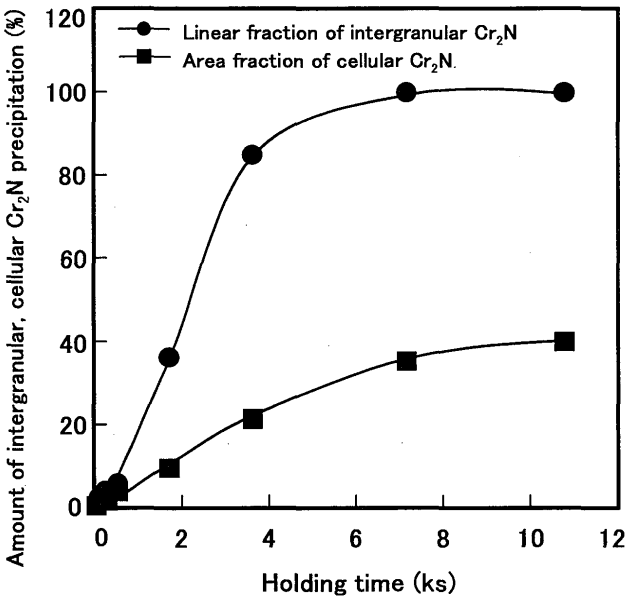


Fig.4 Effect of holding time on amount of intergranular and cellular $Cr_2N$ in specimens aged at 1173K.

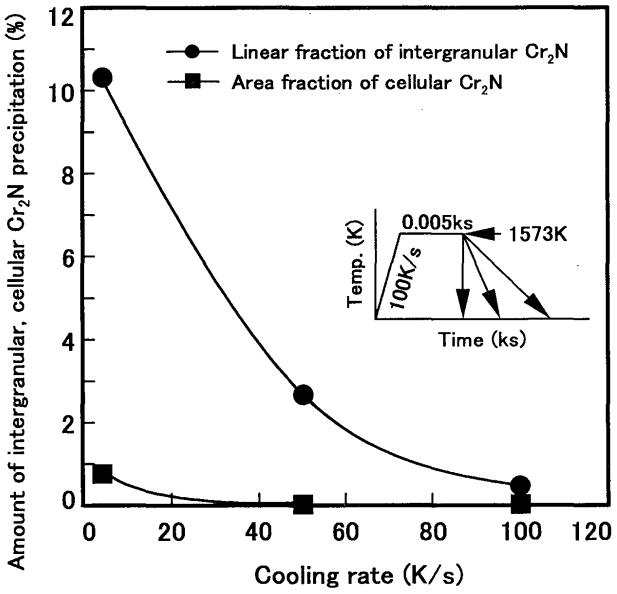


Fig.5 Effect of cooling rate on amount of intergranular and cellular $Cr_2N$ in HAZ.

The linear fraction of intergranular $Cr_2N$ and area fraction of cellular $Cr_2N$ were measured and plotted as function of holding time, as shown in **Fig.4**. These values for grain boundary coverage were determined from image analysis (measurement of the total amount of grain boundary attack) of metallographically prepared samples etched electrolytically with oxalic acid. This result suggests that the grain boundary precipitation of $Cr_2N$ occurred during aging at 1173K, with the degree of $Cr_2N$ coverage on grain boundary increasing with holding time. Nearly 100% of the grain boundaries contained $Cr_2N$ after 7.2ks at 1173K. The area fraction of cellular $Cr_2N$ produced in heat treated specimens during aging at 1173K increased with holding time and reached a maximum of about 40% (total cell fraction, $\gamma$+ $Cr_2N$) after 10.8ks of aging heat treatment. The relationship between the amount of $Cr_2N$ precipitation in the HAZ and the cooling rate during the welding thermal cycle is shown in **Fig.5**. The values of linear fraction of intergranular $Cr_2N$ and area fraction of cellular $Cr_2N$ had a tendency to increase with decreasing cooling rate.

### 3.2 Factors affecting to Charpy impact property

Average Charpy-V impact toughness values of the test material between 293K and 77K are present in **Fig.6**. The impact toughness of high nitrogen containing Ni-free austenitic stainless steel was excellent at room temperature, exceeding 280J. However, impact toughness values tended to decrease with decreasing testing temperature, and ductile-to brittle transition (DBT) behavior was observed. The sharpest decrease occurred between 273K and 250K. Charpy impact test results of high nitrogen containing Ni-free austenitic stainless steel observed in this study were in accordance with earlier investigations for the same type of stainless steels[1,12].

The relationship between impact toughness and amount of $Cr_2N$ precipitation with a variation of cooling rate during the welding thermal cycle is shown in **Fig.7**. The values of absorbed energy of the HAZ tested at room temperature decreased with increasing linear fraction of intergranular $Cr_2N$ and area fraction of

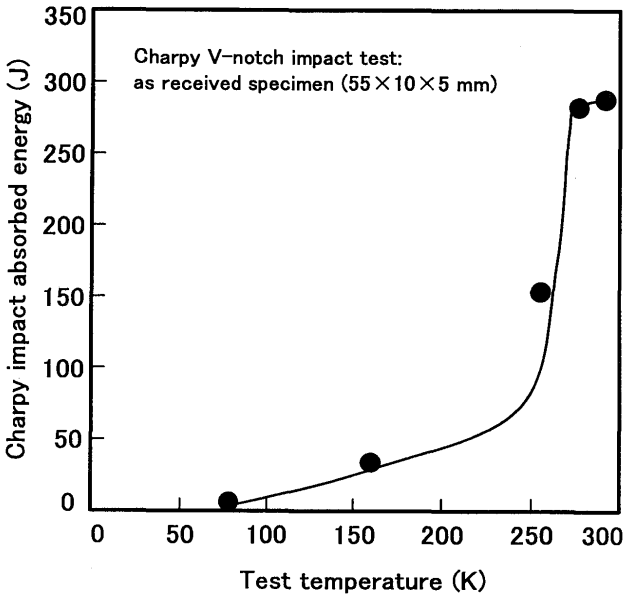


Fig.6 Effect of test temperature on Charpy impact absorbed energy of high nitrogen containing Ni-free austenitic stainless steel

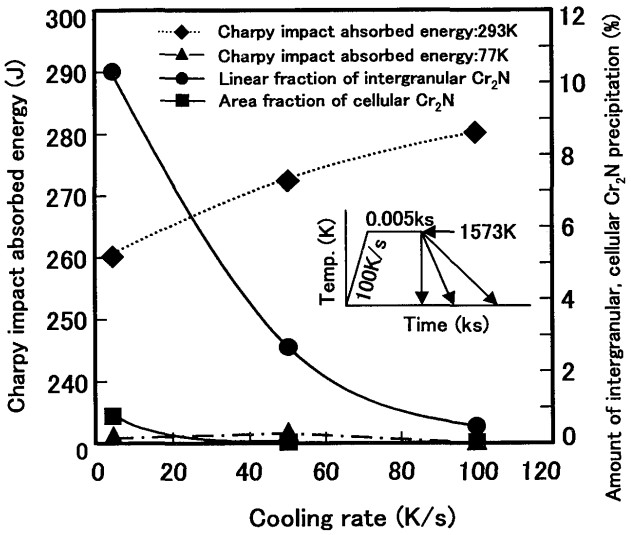


Fig.7 Effect of cooling rate on Charpy impact absorbed energy and amount of intergranular, cellular $Cr_2N$ precipitation.

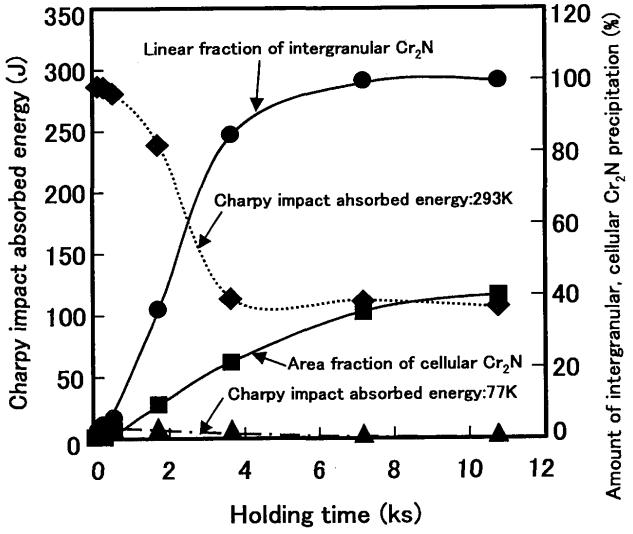


Fig.8 Effect of holding time on Charpy impact absorbed energy and amount of intergranular, cellular $Cr_2N$ precipitation in specimens aged at 1173K.

cellular $Cr_2N$. However, the impact property of the HAZ tested at 77K was not affected by intergranular and cellular $Cr_2N$ precipitation. As shown in **Fig.8**, deleterious effects of $Cr_2N$ precipitation on the room-temperature impact properties occurred more clearly for aging heat treatments than welding thermal cycles. After aging for 3.6ks at 1173K, the absorbed energy decreased to 100J from 280J in the as-received specimen.

SEM micrographs obtained from fractured surfaces of Charpy impact test specimens for as-received material formed at room temperature and 77K are presented in **Fig.9**. The fracture type in room temperature Charpy testing was ductile fracture which occurred as a result of microvoid coalescence (Fig.9 (a) and (b)). On the other hand, the fractured surface at 77K consisted of very flat facets due to transgranular brittle fracture (Fig.9 (c) and (d)). These features suggest that the very poor toughness of high nitrogen containing Ni-free austenitic stainless steel at cryogenic temperature is related to the occurrence of transgranular brittle fracture. **Fig.10** shows SEM fractographs obtained from room temperature Charpy testing of aged specimens at 1173K for 0.03ks and 10.8ks. As shown in Fig.10 (a), the specimen aged at 1173K for 0.03ks was characteristically ductile with a dimple rupture fracture appearance similar to that shown in Fig.9 (a) and (b). However, the fracture surface of the specimen aged at 1173K for 10.8ks contained large areas of grain boundary failure and separation, with transgranular fracture through regions of cellular precipitation (Fig.10 (b)). **Fig.11 (a)** and **(b)** shows SEM fractographs obtained from 77K Charpy testing for aged specimens at 1173K for 0.03ks and 3.6ks, respectively. The fractured surfaces of these aged specimens, regardless of holding time, consisted of very flat facets due to transgranular brittle fracture.

## 4. Discussion

The foregoing results indicated that room temperature impact toughness of the HAZ in high nitrogen containing Ni-free austenitic stainless steel was dramatically decreased with increasing amounts of intergranular and cellular $Cr_2N$ precipitates. Three-point bending test specimens, as shown in **Fig.12**, demonstrate the mechanism of crack nucleation and propagation in aged specimens. Fig.12 (a) shows SEM micrograph obtained from room temperature three-point bending test of an aged specimen at 1173K for 0.18ks. Interfacial separation between intergranular $Cr_2N$ and $\gamma$-matrix creates a crack, which propagate along the grain boundaries. On the other hand, as shown in Fig.12 (b), the microcracks are observed in the cellular $Cr_2N$ precipitates for aged materials at 1173K for 3.6ks. These features suggest that, in the aged specimens, grain boundary failure and separation, with transgranular fracture obtained from the Charpy impact testing at room temperature is mainly caused by the intergranular and cellular $Cr_2N$ precipitates.

For $Cr_2N$ within the cellular phase and intragranular $Cr_2N$, the basal plane of the $Cr_2N$ was found to be parallel to the {111} close-packed planes of the $\gamma$-matrix. It has also been reported that intergranular $Cr_2N$ precipitate has a coherent interface with one grain and an incoherent interface with the other grain[13-15]. If the coherence is not satisfied, the microcracks will easily occur at such interfaces between $Cr_2N$ precipitate and

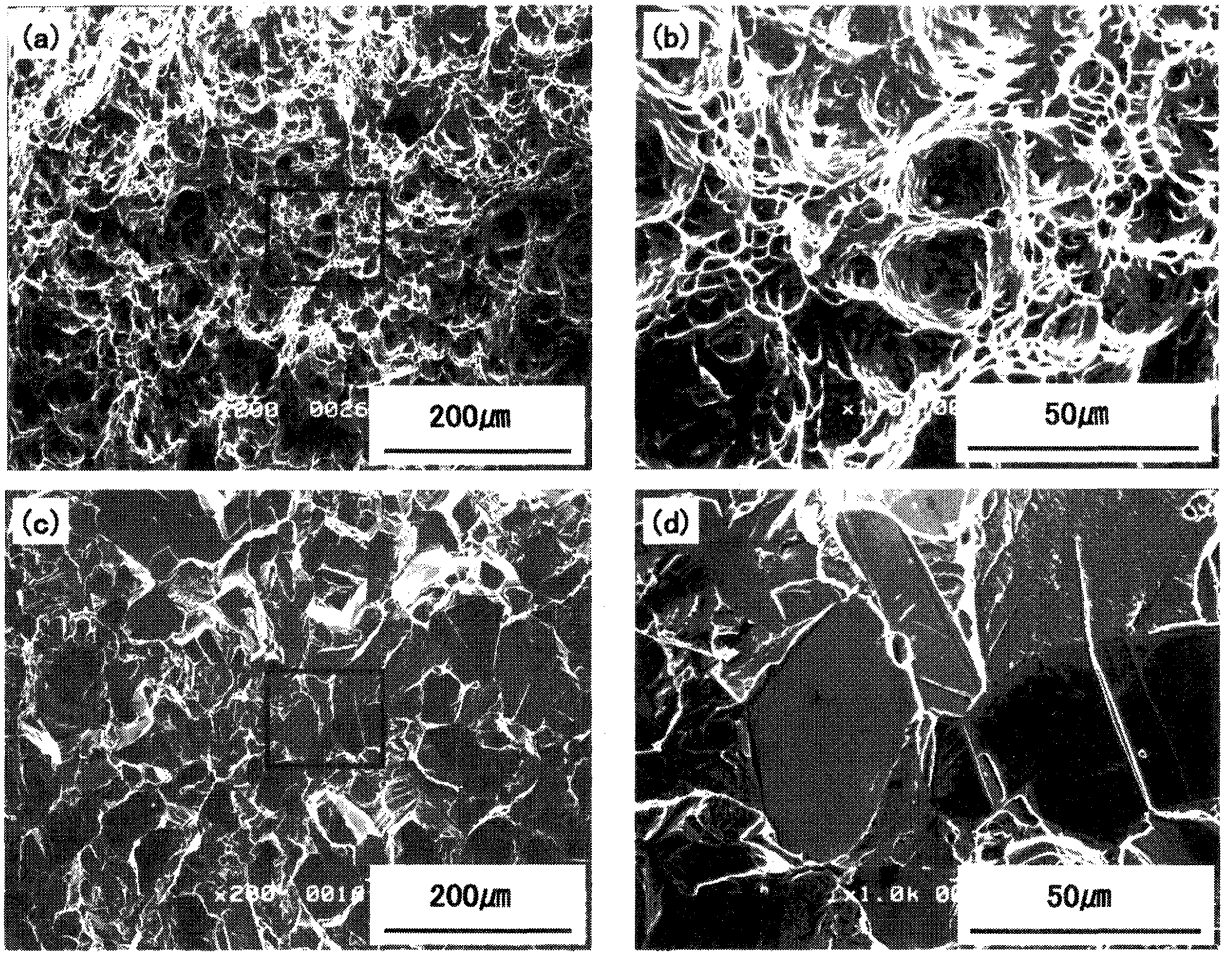


Fig.9 SEM fractographs of Charpy specimens from high nitrogen containing Ni-free stainless steel: (a) Test temperature; 293K, (b) Higher magnification of (a) (c) Test temperature; 77K, (d) Higher magnification of (c).

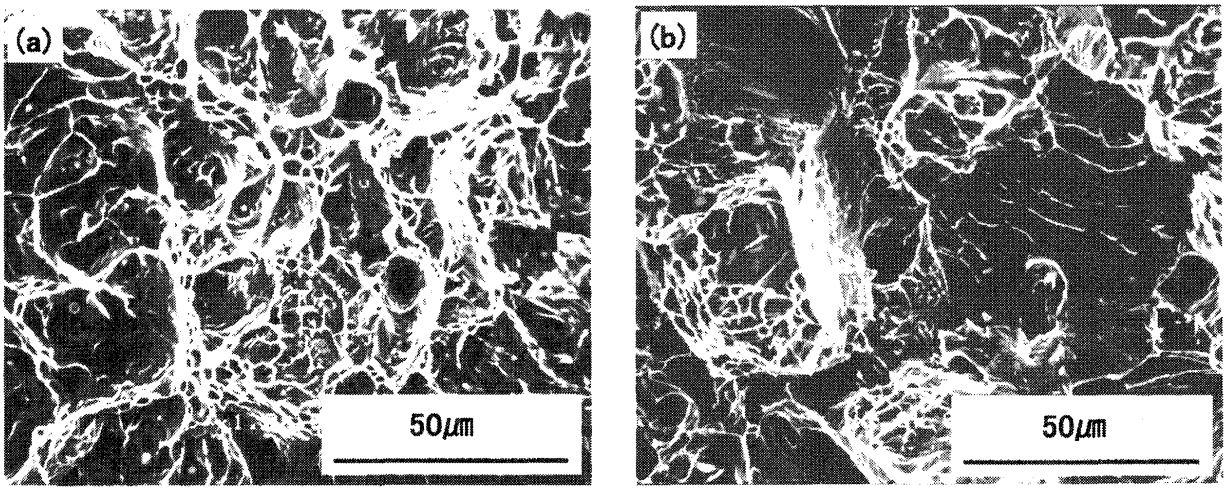


Fig.10 SEM fractographs after Charpy impact test at 293K:
(a) Specimen aged for 0.03ks at 1173K,
(b) Specimen aged for 10.8ks at 1173K.

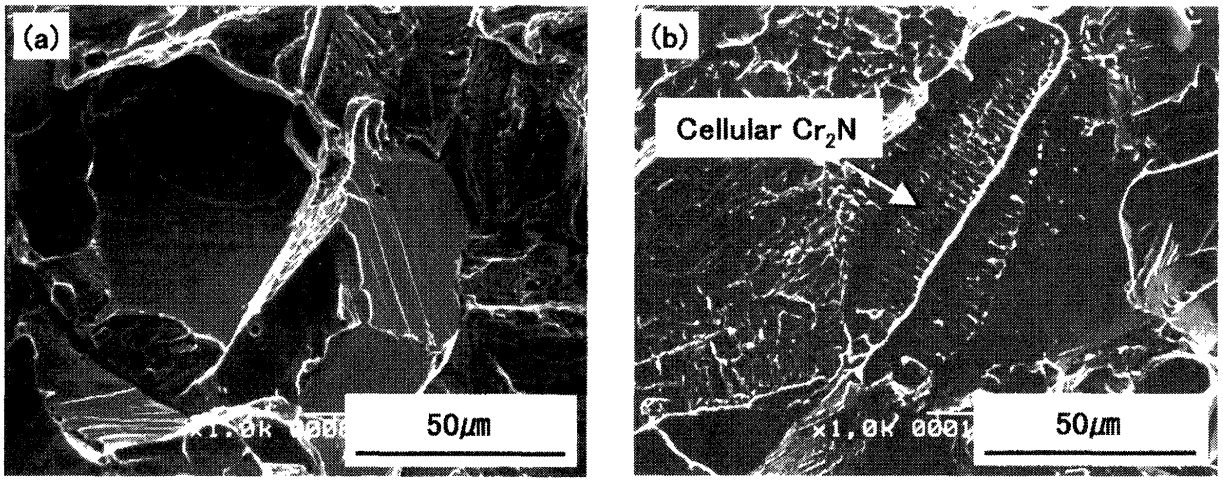


Fig.11 SEM fractographs after Charpy impact test at 77K:
(a) Specimen aged for 0.03ks at 1173K,
(b) Specimen aged for 3.6ks at 1173K.

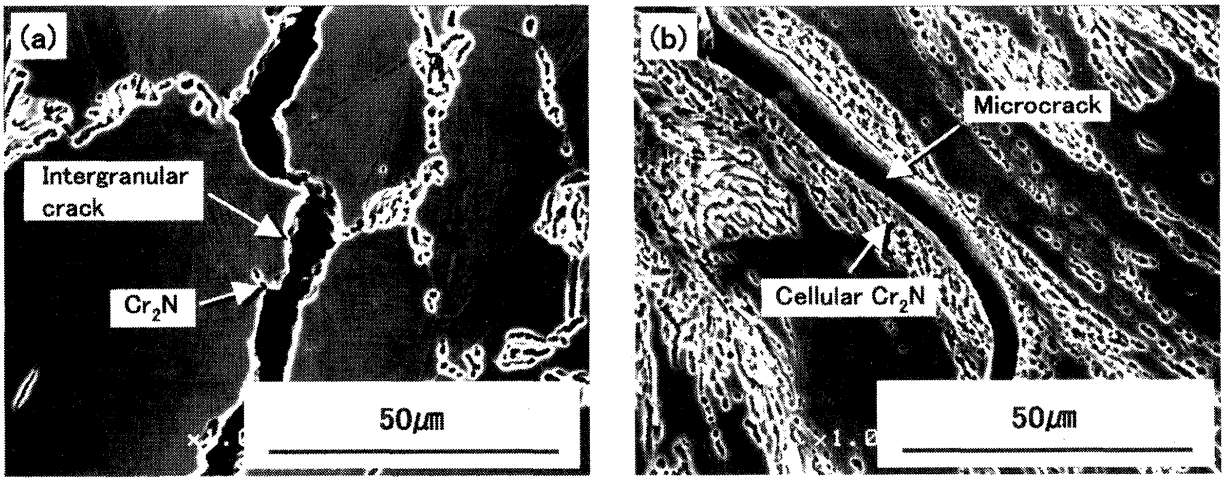


Fig.12 SEM micrographs after bending test at 293K:
(a) Intergranular crack of specimen aged for 0.18ks at 1173K,
(b) Microcrack in cellular of specimen aged for 3.6ks at 1173K.

grain due to reduction of the cohesive strength. Fracture in cellular $Cr_2N$ regions occurs through a mechanism similar to that suggested for the fracture of pearlite in carbon steels[16-18]. Namely, that the cracking of $Cr_2N$ in cellular occurs, by the development of a shear zone in the γ phase to generate cracking in the adjacent $Cr_2N$, coalescence of the small holes at the breaks in the cellular phase, and subsequent failure. Although the fractographic features of the cracking in the cellular $Cr_2N$ precipitate regions (Fig.10 (b)) support this mechanism, more work is necessary to verify the mechanism.

In contrast to the room temperature impact toughness of the HAZ, the interesting fact is that, at 77K, impact toughness of HAZ in high nitrogen containing Ni-free austenitic stainless steel was not much influenced by the intergranular and cellular $Cr_2N$ precipitates. The foregoing results indicated that as-received material, which contained no intergranular and cellular $Cr_2N$ precipitate and had all of the nitrogen present interstitially, failed by the transgranular brittle fracture at cryogenic temperatures. Hence, at 77K, the poor toughness property of HAZ containing intergranular and cellular $Cr_2N$ precipitates can be attributed to the transgranular brittle fracture of the γ-matrix. In recent years, authors[19-22] have discussed the crack propagation behavior of nitrogen containing austenitic stainless steels in terms of alloying, temperature, stacking fault energy, fracture stress, and yield stress. Alloying elements which decrease the stacking fault energy, such as nitrogen and manganese, and increase the DBTT. On the other hand, Nickel increases the stacking fault energy, and decreases the DBTT. High nitrogen containing Ni-free austenitic stainless steel used in the present study will have high

stacking fault energy because of high N and Mn, which results in the transgranular brittle fracture at cryogenic temperature.

## 5. Conclusion

This study is intended to investigate the effect of microstructure on the impact property in the heat-affected zone of high nitrogen containing Ni-free austenitic stainless steel. The main conclusions derived are as follow.

(1) The electron diffraction analysis revealed that the intergranular, cellular and transgranular precipitates are $Cr_2N$ (Hexagonal, a=0.48113nm, c=0.44841nm).

(2) The $Cr_2N$ precipitation showed that the nose of each C curve (i.e., intergranular, cellular, and transgranular $Cr_2N$) was around 1173K. Additionally, $Cr_2N$ precipitation occurred sequentially at grain boundaries, by cellular precipitation, and, finally, by transgranular precipitation within the matrix.

(3) The amount of intergranular and cellular $Cr_2N$ precipitation had a tendency to increase with increasing holding time or decreasing cooling rate.

(4) High nitrogen containing Ni-free austenitic stainless steel exhibited excellent impact toughness at room temperature. At cryogenic temperature, the impact toughness was decreased markedly, and ductile-to-brittle (DBT) transition behavior associated with brittle transgranular fracture was observed.

(5) Intergranular and cellular $Cr_2N$ precipitation reduced the impact property of the HAZ at room temperature. In addition, embrittlement occurred due to grain boundary separation and fracture through cellular precipitation regions, initiated at $Cr_2N$. However, regardless of the amount of intergranular and cellular $Cr_2N$ precipitation, impact toughness values of the HAZ were not observed at cryogenic temperature.

## References


1) Y.Ikegami and R.Nemoto: *ISIJ Int.*, **36**(1996), 855.
2) J.Menzel, W.Kirschner and G.Stein: *ISIJ Int.*, **36**(1996), 893.
3) P.J.Uggowitzer, R.Magdowski and M.O.Speidel: *ISIJ Int.*, **36**(1996), 901.
4) P.J.Uggowitzer, W.F.Bahre, H.Wohlfromm and M.O.Speidel: *Material Science Forum*, **318-320**(1999), 663.
5) Y.Kikuchi, O.kamiya and H.Kobayashi: *Material Science Forum*, **318-320**(1999), 621.
6) I.Woo, T.Horinouchi and Y.Kikuchi: *Testu to Hagane*, **87**(2001), 486.
7) T.Ogawa, K.Susuki and T.Zaizen: *Welding J.*, **64**(1984), 213.
8) J.W.Simmons: *Metall.Trans.*, **26A**(1995), 2085.
9) I.Woo, T.Horinouchi and Y.Kikuchi: *Trans.JWRI*, **29**(2000), 67.
10) H.C.Holm, P.J.Uggowitzer and M.O.Speidel: *Scripta Metall.*, **21**(1987), 513.
11) D.B.Rayaprolu and A.Hendry: *Mater.Sci.Technol.*, **4**(1988), 136.
12) T.Tanaka, M.kikuchi and R.Tanaka: Nippon Kinzoku Gakkaishi, **41**(1977), 1145.
13) M.Kikuchi, M.Kajihara and S.K.Choi: Mater.Sci.Eng., **A146**(1991), 131.
14) D.B.Rayaprolu and A.Hendry: *Mater.Sci.Technol.*, **5**(1989), 328.
15) Y.Tomota, Y.Xia and k.Inoue: *Acta mater.*, **46**(1998), 1577.
16) A.R.Rosenfield, G.T.Hahn and J.D.Embury: *Metall.Trans.*, **3**(1972), 1972.
17) U.Lindborg: *Trans.ASM*, **61**(1968), 500.
18) L.E.Miller and G.C.Smith: *J.Iron and Steel Institute*, **11**(1970), 998.
19) P.Mullner, C.Solenthaker, P.J.Uggowitzer and M.O.Speidel: *Acta metal.mater.*, **42**(1994), 2211.
20) P.M.Adler, G.B.Olson and W.S.Owen: *Metall.Trans.*, **17A**(1986), 1725.
21) V.G.Gavriljuk, A.L.Sozinov, Ju.N.Petrov and Yu.A.Polushkin: *Acta metal.mater.*, **46**(1998), 1157.
22) J.Ishizaka, K.Orita and K.Terao: *Testu to Hagane*, **78**(1992), 1846.